J. Fluid Mech. (1984), *vol.* 141, *pp.* 249–264
Printed in Great Britain

Volume-cycled oscillatory flow in a tapered channel

By JAMES B. GROTBERG

Department of Engineering Sciences and Applied Mathematics, The Technological Institute, Northwestern University, Evanston, Illinois 60201, and Department of Anesthesia, Northwestern University Medical School, Chicago, Illinois 60611

(Received 1 July 1983 and in revised form 8 December 1983)

Oscillatory viscous flow in a tapered channel is analysed under conditions of fixed stroke volume. A lubrication theory is developed for small taper and the general result is steady bidirectional drift and an induced steady pressure gradient. The characteristics of the drift profiles change significantly as the Womersley parameter is increased. For large values difficulties arise in the matched asymptotics method which are resolved by introducing a steady drift layer that is much thicker than the Stokes layer. This double boundary layer does not arise in pressure-cycled oscillations. Both Eulerian and Lagrangian drift are examined. The results are compared qualitatively to experimental observations which primarily focus on the application to ventilation in the lung.

1. Introduction

A common device used to assist respiration during surgical procedures or in intensive-care settings is the mechanical ventilator. Typically, ventilators deliver tidal breaths on the order of 600–800 cm^3 at a rate of 8–12 breaths per minute for an adult. This pattern mimics normal respiration. The tidal volumes are 4–6 times larger than the lung dead space, which is the volume of conducting airways where no gas exchange occurs. Therefore transfer of oxygen and carbon dioxide is dominated by penetration of the gas bolus into the alveolar space. A relatively new method of mechanical ventilation, however, utilizes tidal breaths that are much smaller than the dead space, but driven at high frequencies, 5–30 Hz. This pattern mimics panting. Experiments on dogs by Slutsky *et al.* (1980), Bohn *et al.* (1980), McEvoy *et al.* (1982) and on humans by Butler *et al.* (1980) demonstrate favourable gas exchange with this method. Clearly, the simple bulk penetration of tidal breaths is not responsible for this result. A major feature of high-frequency ventilation (HFV) is the oscillatory gas flow in the airways and particularly at their bifurcations. Haselton & Scherer (1982) have examined piston-driven oscillatory flow of a liquid in a branching Y-tube. Their studies show that periodic cycling of a constant stroke volume induces steady axial drift of marked fluid which is bidirectional. Several values of the Womersley parameter α and the Reynolds number are investigated. Further details of this study were presented in Scherer & Haselton (1982), where its possible importance as a mode of gas exchange and aerosol deposition is discussed. They suggest that a probable explanation of the drift is the difference in axial velocity of profiles between inspiratory and expiratory flow at the bifurcation. Pressure measurements have been made in intact animals during HFV by Simon, Weinmann & Mitzner (1982), who measured time-averaged alveolar and airway (trachea) pressures in dogs. They found that, for high-enough frequencies, mean alveolar pressure exceeds mean airway pressure, and the magnitude of this difference increases with frequency. Other

investigators (Gavriely 1983 personal communication) have observed similar steady pressure gradients indirectly. They note that, while the mean airway pressure is held constant during HFV in dogs, the lungs inflate to a larger mean volume. The appearance of a steady pressure gradient from purely oscillatory forcing strongly suggests nonlinear flow phenomena which airway bifurcations can provide. A steady pressure gradient indicates the presence of a steady flow, such as the bi-directional streaming discussed above. Hence there is some evidence linking tube experiments to animal experiments concerning the importance of steady streaming in HFV.

A detailed theoretical analysis of velocity profiles for oscillating flow in the vicinity of an airway bifurcation is a formidable task. Complications of secondary swirl flows, vortex formation, separation, turbulence and entrance effects are too difficult to handle with the three-dimensional geometry. However, a notable feature of airway geometry is that the cross-sectional area of a parent airway gradually increases by roughly 20 % to match the total cross-sectional area of the daughters. This transition starts at roughly one-third of the airway length and is completed just prior to the carina as noted in measurements of dog airways by Schreck (1972). The mean slope ϵ of a single airway wall may be estimated by the ratio of its total change in mean radius to its total length. From Schreck (1972) and from human data by Horsefield & Cumming (1967), the upper bound of this parameter is approximately $\epsilon \leqslant 0.1$. The straight Y-tubes used in the above experiments also possess a region of increasing cross-sectional area, starting at the take-off of the daughter tubes and ending at the carina. The corresponding mean slope appears to be $\epsilon \approx 0.7$.

As a first approximation to oscillatory flow at a bifurcation, a model is presented in §2 of a two-dimensional channel segment with slowly increasing depth. Earlier versions of this model appeared in Grotberg (1983*a*, *b*). The fluid contained inside the channel oscillates at a prescribed stroke volume and frequency and the general result is an induced steady, bidirectional drift and steady pressure gradient. This differs significantly from the work of Hall (1974), who considers oscillatory flow in a tube of slowly varying cross-section. Hall prescribes an oscillating pressure difference of constant amplitude. Under these conditions when frequency is increased the amplitude of motion, that is, fluid speeds and stroke volume, monotonically decrease. In our problem, however, stroke volume is fixed, so unsteady fluid speeds increase with frequency. The stroke amplitude A, which is a ratio of the local oscillatory displacement amplitude to the local tube radius, now becomes an important parameter which is not fixed in Hall's work. The product $\epsilon A = \lambda$ is a modified amplitude parameter which determines the behaviour of the steady bi-directional drift. It plays a role similar to the torsional oscillation amplitude in Jones & Rosenblat (1969) and the linear oscillation amplitude in Stuart (1966). The analogy includes restrictions on the asymptotic series developed in §§3 and 4, such that $\epsilon A\alpha^2 \ll 1$ in the low-to-middle-frequency range ($\alpha \leqslant O(1)$). It also includes similarities in the high-frequency limit ($\alpha \gg 1$). In this limit the method of matched asymptotic expansions adequately describes the periodic motion to leading order by appropriately scaling the boundary-layer coordinate on the Stokes-layer thickness δ_s. It fails, however, to handle the steady drift that arises at higher order. Rapid changes in the steady-drift velocity profile occur over a larger distance from the wall than the Stokes layer. A second boundary-layer coordinate based on the drift-layer thickness $\delta_D = \delta_s/\lambda$ must be introduced into the analysis and eventually leads to the desired solution. This thicker drift layer does not appear in Hall's analysis because of the inverse relationship between α and velocity. The large-α solution corresponds to large values of the steady streaming Reynolds number $R_s = \alpha^2 A$. A simplified version of

the method of Fettis (1956) as outlined in Stuart is used to solve this double boundary-layer problem in §5. The steady Lagrangian drift is computed in §6 and contrasted to the corresponding Eulerian drift for low and high frequencies. Some comparisons are made between the theoretical predictions and the experimental results of Haselton and Scherer. The induced steady pressure gradient is treated in §7 and compared with the experimental observations. Some concluding remarks and criticisms are offered in §8.

2. Problem formulation

We shall examine the two-dimensional flow of an incompressible fluid with density ρ and kinematic viscosity ν. The fluid is confined by a section of rigid channel walls whose position $y^* = \pm W^*(x^*)$ is symmetric with respect to the axial coordinate x^*, where $0 < x^* < L$. The channel half-depth at the origin is $W^*(0) = b$, and we define the dimensionless parameter

$$\epsilon = (W^*(L) - W^*(0))/L \tag{2.1}$$

as a measure of the slope of W^*. Oscillatory fluid motion is imposed by specifying the periodic volume flow rate in the channel, that is, the local channel stroke volume, V and frequency $\omega = 2\pi f$. V is defined by

$$V = 2b \int_{T_1}^{T_2} \int_0^{W^*} u^* \, \mathrm{d}y^* \, \mathrm{d}t^*, \tag{2.2}$$

where the time interval T_1 to T_2 coincides with a full unidirectional stroke and $T_2 = T_1 + \pi/\omega$. For convenience we define a displacement length $d = V/2b^2$. The parameter d reflects the amplitude of the fluid oscillations. An appropriate indicator of the corresponding fluid velocity amplitudes is then defined as $U = \omega d$.

The fluid motion is governed by the Navier–Stokes equations given in the following dimensionless form:

$$\alpha^2 u_t + \alpha^2 \lambda (u u_x + v u_y) = -\alpha^2 \lambda p_x + \epsilon^2 u_{xx} + u_{yy}, \tag{2.3}$$

$$\epsilon^2 (\alpha^2 v_t + \alpha^2 \lambda (u v_x + v v_y)) = -\alpha^2 \lambda p_y + \epsilon^2 (\epsilon^2 v_{xx} + v_{yy}), \tag{2.4}$$

and by mass conservation for incompressible fluids

$$u_x + v_y = 0. \tag{2.5}$$

The dimensionless variables are defined by

$$u = \frac{u^*}{U}, \quad \epsilon v = \frac{v^*}{U}, \quad p = \frac{p^*}{\rho U^2}, \quad t = \omega t^*, \quad x = \frac{\epsilon x^*}{b}, \quad y = \frac{y^*}{b}, \tag{2.6}$$

and the dimensionless parameters are

$$A = \frac{d}{b}, \quad \alpha^2 = \frac{\omega b^2}{\nu}, \quad \lambda = \epsilon A, \tag{2.7}$$

where an asterisk indicates dimensional quantities. α is the Womersley parameter and A is the amplitude parameter. The boundary conditions of no slip at the stationary walls simplify for the symmetric channel and are

$$u = v = 0 \quad \text{on} \quad y = W(x), \tag{2.8a, b}$$

$$u_y = v = 0 \quad \text{on} \quad y = 0 \tag{2.8c, d}$$

3. Method of solution

We are interested in a channel with small slope $\epsilon \ll 1$, and utilize this assumption in a lubrication theory to solve the governing equations (2.3)–(2.5) and the boundary conditions (2.8). The choices of the x- and v-scalings in (2.7) were made in anticipation of this method. It is convenient to eliminate pressure as a variable and combine (2.3) and (2.4) in a stream-function equation. Neglecting terms $O(\epsilon^2)$ we arrive at the following:

$$\alpha^2\psi_{yyt} - \psi_{yyyy} + \alpha^2\lambda(\psi_y\psi_{xyy} - \psi_x\psi_{yyy}) = 0, \tag{3.1}$$

where $\lambda = \epsilon A \ll 1$, and A is a fixed order-unity quantity. The x- and y-components of velocity are respectively

$$u = \psi_y, \quad v = -\psi_x. \tag{3.2}$$

The boundary conditions become the equivalent statements in terms of the stream function:

$$\psi_y = \psi_x = 0 \quad \text{on} \quad y = W(x), \tag{3.3a, b}$$

$$\psi = \psi_{yy} = 0 \quad \text{on} \quad y = 0. \tag{3.3c, d}$$

Since (3.3a, b) ensure that $\nabla\psi = \mathbf{0}$ on the wall, then $\psi(y = W)$ depends on t only and represents the oscillating volume flow rate between the midplane $\psi = 0$ and the wall. It is computationally easier to replace (3.3b) with the equivalent constraint

$$\psi = \tfrac{1}{4}e^{it} + \text{c.c.} \quad \text{on} \quad y = W, \tag{3.3e}$$

which corresponds dimensionally to (2.2) when integrated over one half-cycle. The abbreviation c.c. denotes complex conjugate. We solve (3.1) by expanding the stream function for $\lambda \ll 1$:

$$\psi = \psi_0 + \lambda\psi_1 + O(\lambda^2). \tag{3.4}$$

By inserting (3.4) into (3.1) and collecting terms of like power in λ, the leading-order problem reduces to the linear equation

$$\alpha^2\psi_{0yyt} - \psi_{0yyyy} = 0, \tag{3.5}$$

and the boundary conditions are the same as (3.3) with ψ replaced by ψ_0. The solution to this system is readily found by separation of variables:

$$\psi_0 = (a_0(x)\sinh\sigma y + b_0(x)\,y)\,e^{it} + \text{c.c.}, \tag{3.6}$$

where the x-dependent functions are governed by the prescribed wall shape

$$a_0(x) = \tfrac{1}{4}(\sinh\sigma W - \sigma W\cosh\sigma W)^{-1}, \quad b_0(x) = -\sigma a_0\cosh\sigma W. \tag{3.7}$$

The complex parameter σ is defined as $\sigma = \alpha(1+i)/\sqrt{2}$. At this order, only periodic motion occurs. The next-order problem will contain products of the derivatives of ψ_0, which lead, in general, to periodic terms proportional to e^{i2t} and also to steady terms. We will focus our attention on the latter. At $O(\lambda)$ (3.1) has the form

$$\alpha^2\psi_{1yyt} - \psi_{1yyyy} = \alpha^2(\psi_{0x}\psi_{0yyy} - \psi_{0y}\psi_{0xyy}), \tag{3.8}$$

subject to the $O(\lambda)$ boundary conditions, which are the homogeneous version of (3.3). Of particular concern is the steady-state component of (3.8). After substituting (3.6) into (3.8), we find the $O(\lambda)$ steady correction to be

$$\psi_1^s(x, y) = a_1(x, y) + b_1(x)\,y + c_1(x)\,y^3 + \text{c.c.}, \tag{3.9}$$

Airway generation	b_n (cm)	α_n	S_n (cm^2)	d_n	λ_n
$n = 0$	0.90	18.4	2.54	19.6	1.09
1	0.61	12.4	2.33	21.4	1.75
3	0.28	5.73	2.00	25.0	4.46
5	0.17	3.47	3.11	16.1	4.73
10	0.065	1.33	13.4	3.73	2.87
15	0.033	0.675	113	0.44	0.667
20	0.023	0.471	1600	0.031	0.067
23	0.021	0.430	11800	0.004	0.010

TABLE 1. Estimates of the parameters α and λ for several airway generations. A tidal volume of 50 cm^3 at a rate of 10 Hz is assumed. The stroke amplitude d is calculated from the tidal volume and total cross-sectional area at the generation, i.e. $d_n = 50/S_m$ and $A_n = b_n/d_n$. The airway radius is substituted for b_n. $\epsilon = 0.05$. (From Weibel (1963).)

with the definitions

$$a_1(x,y) = -\mathrm{i}\sigma a_0 \bar{a}_0' (\sinh \sqrt{2}\,\alpha y - \mathrm{i}\sin\sqrt{2}\,\alpha y) - 2\mathrm{i}(4a_0\bar{b}_0' + a_0'\bar{b}_0)\sinh\sigma y + 2\mathrm{i}\sigma a_0 \bar{b}_0' y\cosh\sigma y, \tag{3.10a}$$

$$b_1(x) = -c_1 W^2 - a_1(x,W)/W, \tag{3.10b}$$

$$c_1(x) = \tfrac{1}{2}W^{-3}(a_1(x,W) - W a_{1y}(x,W)). \tag{3.10c}$$

In (3.10) a prime indicates differentiation with respect to x and an overbar denotes complex conjugate. Further calculations of ψ to higher order show that $\lambda\psi_1 \sim \alpha^2\lambda$ and $\lambda^2\psi_2 \sim \alpha^4\lambda^2$. The asymptotic series is only valid if the product $\alpha^2\lambda \ll 1$. As the Womersley parameter α is varied we expect good approximation as long as λ is small enough. In the bronchial network, the corresponding values of these parameters are listed in table 1 for representative frequencies and tidal volumes. The airway radius is replaced by b and the stroke distance d is calculated from plug flow and the total cross-sectional area at the given airway generation.

4. The Eulerian steady drift, $\alpha \leqslant O(1)$

The results of §3 predict steady drift even though the net volume flux is zero. Hence, in the case where the wall gradually flares as x increases, similar to an airway, we must have bi-directional drift of fluid whose amplitude is linearly proportional to λ at this order. The Eulerian steady axial drift velocity is plotted in figure 1(*a*) for several values of α with $\lambda = 0.002$. Note that the integral of this velocity over the half-width must be zero by continuity. The steady drift is positive, toward the larger end, for fluid near the centreline, and negative, toward the smaller end, for fluid near the wall. The drift amplitude increases with α, while the single crossover value of y remains essentially constant. In figure 1(*b*) larger values of α give quite a different picture. The midline velocity decreases as α increases such that the $\alpha = 10$ curve has negative drift, which becomes even more negative as α is increased to 20. Along with this reversal is the appearance of a second crossover point resulting in negative drift near the wall and near the midline, but positive drift in an intermediate region. The

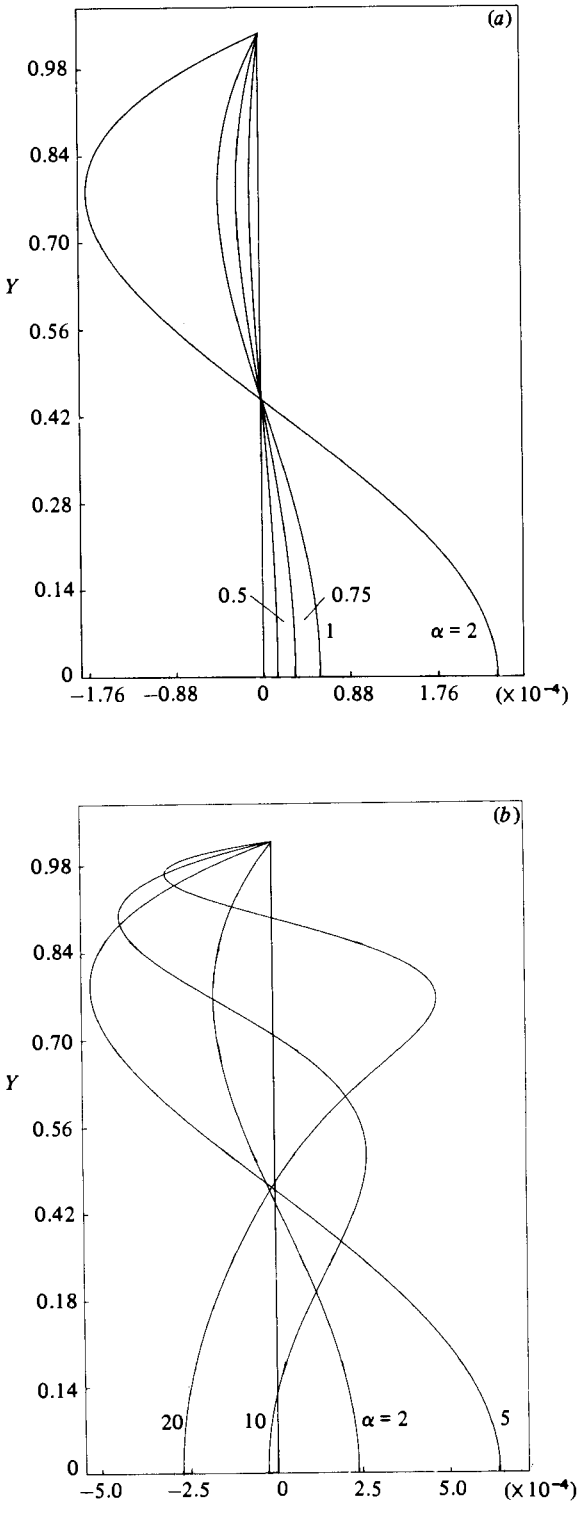

FIGURE 1. Eulerian axial drift velocity profile for several values of $\alpha \leqslant O(1)$ and $\alpha^2\lambda \ll 1$; $\lambda = 0.002$.

rather small choice of λ for figures 1 (a, b) satisfies the requirement that $\lambda \ll 1/\alpha^2$ for the most restrictive case illustrated, $\alpha = 20$. A separate analysis for high-frequency oscillations, $\alpha \gg 1$, is outlined in §5, where this restriction on λ is removed and replaced by the less severe constraint $\lambda \ll 1$. We shall see that the qualitative features of the three drift regions presented here overlap with the following analysis for large α.

The channel shape used is

$$W^* = b \quad (0 \leqslant x^* \leqslant \tfrac{1}{3}L), \tag{4.1a}$$

$$W^* = b + \frac{k}{b}(x^* - \tfrac{1}{3}L)^2 \quad (\tfrac{1}{3}L \leqslant x^* \leqslant L), \tag{4.1b}$$

where the aspect ratio is $L/b = 6$, $k = 0.1$ and $\epsilon = 0.267$ according to (2.1). For this example and those that follow, $x^* = 2L/3$.

5. The Eulerian steady drift, $\alpha \gg 1$: the double boundary layer

In this section we employ the method of matched asymptotic expansions to investigate (3.1) in the limit of $\alpha \to \infty$. This flow has some similarities to oscillatory flow in a straight tube or channel, such as development of an inviscid core region, which oscillates like a fluid plug, and a Stokes layer near the rigid boundary. However, it differs by the appearance of a drift boundary layer near the wall which is much thicker than the Stokes layer.

We proceed by first examining the inviscid core or outer region with dependent variables Ψ, U, V and P. Dividing (3.1) by α^2 and taking the outer limit $\alpha \to \infty$ leaves us with the inviscid equation

$$\Psi_{yyt} + \lambda(\Psi_y \Psi_{xyy} - \Psi_x \Psi_{yyy}) = 0. \tag{5.1}$$

An expansion of Ψ in powers of λ can be solved as before, where Ψ satisfies only the midline boundary conditions (3.3c, d). Omitting details of the calculation, the expansion is found to be

$$\Psi = K_0(x)\, y\, e^{it} + \lambda(K_1(x)\, y\, e^{i2t} + K_2(x)\, y) + \text{c.c.} + O(\lambda^2). \tag{5.2}$$

$K_0(x)$ will be determined in the matching procedure, while the steady x-direction velocity $U^s = \lambda K_2(x)$ in the outer region will be determined by the integral mass-balance equation. It will be necessary to calculate the large-α pressure gradient from (3.1) and (2.3). By expanding the pressure gradient as

$$P_x = \frac{1}{\lambda}(P_{0x} + \lambda P_{1x} + O(\lambda^2)) + O\left(\frac{1}{\alpha}\right) \tag{5.3}$$

we find from the y-component of momentum that $P_y = 0$ to this order. From the x-component of momentum the pressure gradient is determined to be

$$P_{0x} = -iK_0 e^{it} + \text{c.c.}, \quad P^s_{1x} = -K_0 \bar{K}_0' + \text{c.c.} \tag{5.4a, b}$$

The unsteady component of P_1 is of no concern so is omitted here. The steady component P^s_{1x}, as well as the unsteady components, are transmitted to the Stokes layer without modification since $P_y = 0$ throughout. A more detailed discussion of the pressure gradient is given in §7.

The boundary layer or inner region is examined by using the variable transformation

$$\xi = x, \quad \eta = \alpha(W(x) - y), \tag{5.5}$$

which is inserted into (3.1) using the appropriate chain rule for partial derivatives. The inner dependent variables are ϕ, u, v and P. The limiting form for large α becomes

$$\phi_{\eta t} - \phi_{\eta\eta\eta} = (P_{0x} + \lambda P_{1x}) + \lambda(\phi_\eta \phi_{\xi\eta} - \phi_\xi \phi_{\eta\eta}) + O\left(\frac{1}{\alpha}\right). \tag{5.6}$$

$\phi(\xi, \eta, t) = \alpha\psi(x, y, t)$ must satisfy the boundary conditions at the wall

$$\phi_\eta = 0, \quad \phi = \tfrac{1}{4}\alpha e^{it} + \text{c.c.} \quad \text{on} \quad \eta = 0. \tag{5.7}$$

If we expand ϕ in powers of λ, that is

$$\phi = \phi_0 + \lambda\phi_1 + O(\lambda^2) + O\left(\frac{1}{\alpha}\right), \tag{5.8}$$

and insert (5.8) into (5.6), we find the leading-order term

$$\phi_0 = \left(\frac{K_0}{\gamma}(1 - e^{-\gamma\eta} - \gamma\eta) + \tfrac{1}{4}\alpha\right) e^{it} + \text{c.c.} \tag{5.9}$$

The matching condition at this order, for both x- and y-components of velocity, shows $K_0 = 1/4W$. A composite solution of the velocity field, valid for the entire flow regime to leading order, is obtained from (5.2) and (5.9):

$$\hat{u}_0 = \frac{1}{4W}(1 - e^{-\gamma\eta})\, e^{it} + \text{c.c.}, \quad \hat{v}_0 = \frac{W'}{4W}\left(\frac{y}{W} - e^{-\gamma\eta}\right) e^{it} + \text{c.c.}, \tag{5.10a, b}$$

where $\gamma = (1+i)/\sqrt{2}$. Proceeding to next order, the steady component of ϕ_1 from (5.8) is found to be

$$\phi_1^s = \frac{-W'}{16\sqrt{2}\,W^3}\{\tfrac{1}{2}(1-i)\, e^{-\sqrt{2}\eta} + (5 + i(3+\sqrt{2}\,\eta))\, e^{-\gamma\eta} + (1-i)\, e^{-\bar{\gamma}\eta}\} + F_1(\xi) + G_1(\xi)\,\eta + H_1(\xi)\,\eta^2 + \text{c.c.} \tag{5.11}$$

It is here that the asymptotic method breaks down for fixed-amplitude oscillations. $F_1(\xi)$ and $G_1(\xi)$ are derived by satisfying (5.7), but H_1 is not determinable. In the limit as $\eta \to \infty$ we must be able to match the steady Stokes-layer velocities to the outer region. The least-singular case would be to choose $H_1 = 0$, as done by Stuart (1966) and by Jones & Rosenblat (1968). Then the dominant term in (5.11) leads to the following steady velocities which must be matched to the drift $K_2(x)$ in the inviscid core:

$$\lim_{\eta\to\infty} u_1^s = -\lim \phi_{1\eta}^s = -G_1(\xi) + \text{c.c.} = \frac{3W'}{16W^3} + \text{c.c.}, \tag{5.12a}$$

$$\lim_{\eta\to\infty} v_1^s = -\lim W'\phi_{1\eta}^s = \frac{3(W')^2}{16W^3} + \text{c.c.} \tag{5.12b}$$

The matching cannot be done directly, essentially because the dimensionless Stokes-layer thickness $\delta_s = (\nu/b^2\omega)^{\frac{1}{2}}$ is an inappropriate lengthscale for the steady-drift phenomena. Instead, we shall see that the drift-velocity profile undergoes rapid changes in the y-direction within a larger distance $\delta_D = \delta_s/\lambda$ from the wall, where $\lambda \ll 1$ by assumption. It must do this in order to satisfy both the no-slip condition and the zero-mean-flux condition. Hall's (1974) analysis does not have this latter constraint, so his Stokes layer matches directly to the core drift. No double boundary layer develops in that pressure-cycled oscillatory flow.

We approach this problem in the manner of Stuart by expressing ϕ as

$$\phi = \hat{\phi} - \eta U_0(\xi, t) + \Phi(\xi, \eta, t), \tag{5.13}$$

and inserting (5.13) into (5.6) and (5.7). The first two terms of (5.13) will balance the pressure gradient in (5.6). The remaining relationship for Φ is simplified by separating Φ into steady and periodic components:

$$\Phi = \Phi^{\mathrm{s}} + \Phi^{\mathrm{p}}. \tag{5.14}$$

It is possible, then, to time average the boundary-layer equation, neglect interacting terms of Φ^{s} and Φ^{p}, and arrive at a decoupled equation for Φ^{s} only:

$$\Phi^{\mathrm{s}}_{\eta\eta\eta} + \lambda(\Phi^{\mathrm{s}}_{\xi\eta}\Phi^{\mathrm{s}}_{\eta} - \Phi^{\mathrm{s}}_{\xi}\Phi^{\mathrm{s}}_{\eta\eta}) = 0. \tag{5.15}$$

Rescaling the y-variable in the drift-layer thickness δ_{D} leads to the equation we are seeking, which is devoid of parameters:

$$\chi_{\zeta\zeta\zeta} - \chi_{\xi\zeta}\chi_{\zeta} + \chi_{\xi}\chi_{\zeta\zeta} = 0, \tag{5.16}$$

where we define the new boundary-layer coordinate and stream function as

$$\zeta = \lambda\eta, \quad \chi(\xi, \zeta) = -\Phi^{\mathrm{s}}(\xi, \eta) \tag{5.17}$$

respectively. The function χ must satisfy three boundary conditions

$$\chi = 0 \quad \text{on} \quad \zeta = 0, \tag{5.18a}$$

$$\lim_{\zeta\to 0}\chi_{\zeta} = \lim_{\eta\to\infty} u_1^{\mathrm{s}} = \frac{3W'}{16W^3} + \text{c.c.}, \tag{5.18b}$$

$$\lim_{\zeta\to\infty}\chi_{\zeta} = K_2(x) + \text{c.c.}, \tag{5.18c}$$

which are, in order, the zero-steady-mass-flow condition, the matching of the Stokes-layer solution to the drift layer, and the matching of the drift layer to the inviscid core flow. A simple, representative solution to (5.16) and (5.18) is available by the method of Fettis (1956). If we pick a wall shape that is approximately parabolic, as in §4, then the W-dependent function in (5.12a, b) can be written as

$$G_1(\xi) + \text{c.c.} \approx -b^2\xi, \tag{5.19a}$$

while a similar form is expected for K_2:

$$K_2(\xi) + \text{c.c.} \approx -c^2\xi. \tag{5.19b}$$

An approximate solution to this system is

$$\chi(\xi, \zeta) \approx \frac{b^2 + c^2}{a}\xi(1 - \mathrm{e}^{-a\zeta}) - c^2\xi\zeta, \tag{5.20}$$

in which $a^2 = b^2 + c^2$. In the external-flow problem treated by Stuart, the steady drift matches to zero velocity as $\zeta \to \infty$. That case is equivalent to setting $c = 0$, which would render (5.20) an exact solution to (5.16). Here we consider (5.20) as a first approximation for small c. The composite solution to the steady-drift problem can now be written as

$$\hat{u}^{\mathrm{s}} = \lambda(-\phi^{\mathrm{s}}_{1\eta} + \chi_{\zeta} - b^2\xi) + O(\lambda^2) + O\left(\frac{1}{\alpha}\right). \tag{5.21}$$

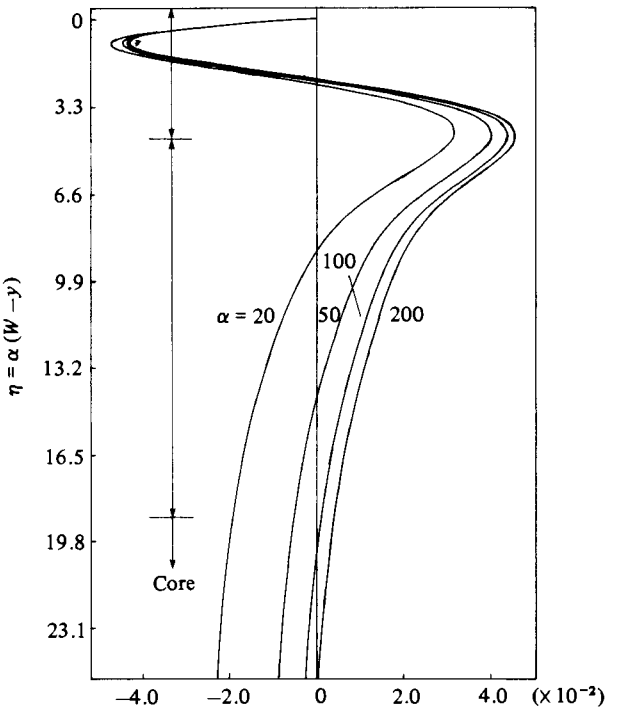

FIGURE 2. Eulerian axial drift-velocity profile for several values of $\alpha \gg 1$; $\lambda = 0.3$.

The remaining unknown function in (5.19*b*) is solved by the integral mass-balance equation for the steady Eulerian velocity:

$$\int_0^W \hat{u}^s \, dy = 0. \tag{5.22}$$

A graph of $\hat{u}^s$ appears in figure 2 plotted as a function of η, and for $\lambda = 0.3$. Note that the wall position is at $\eta = 0$. Qualitatively we see that in the Stokes layer there is negative drift nearest the wall which rapidly reverses as η increases to become positive drift near its outer edge. This is expected from (5.12*a*) when $W' > 0$. The curves then reverse again for larger η and approach asymptotically the inviscid core steady drift U_1^s, which has a small negative value. This is consistent with the assumption of small c. The two boundary-layer thicknesses are denoted and it is clear that this approximation improves as α increases. The three regions of drift and two crossover points are qualitatively similar to the analysis in §4. The steady positive jet toward the wider end of the channel separates a smaller negative Stokes-layer jet from a negative core drift which is smaller still.

6. The Lagrangian steady drift

The actual steady motion of fluid particles in the Lagrangian reference frame may be calculated from the Eulerian velocity fields derived in §§4 and 5. The Eulerian velocities are a basic component of the convection–diffusion equation which ultimately

will govern transport of gas species in the HFV application. The computed Lagrangian velocities may be correlated to experiments which follow fluid-particle motion, such as those by Haselton and Scherer. The Lagrangian velocity vector is the time derivative of the fluid mapping $\boldsymbol{X}(\boldsymbol{X}_0, t)$, where $\boldsymbol{X}_0$ is a reference position. We expand the mapping by the relation

$$\boldsymbol{X} = \boldsymbol{X}_0 + \lambda \boldsymbol{X}_1(\boldsymbol{X}_0, t) + \lambda^2 \boldsymbol{X}_2(\boldsymbol{X}_0, t) + O(\lambda^3), \tag{6.1}$$

which is true for $\lambda \ll 1$ on the basis of small A, that is, $\boldsymbol{X} = \boldsymbol{X}_0$ when $A = 0$. The corresponding expansion for Lagrangian velocity, simply the time derivative of (6.1), is related to the previous Eulerian velocity expansions, denoted in general by $\boldsymbol{u}(\boldsymbol{x}, t) = \boldsymbol{u}_0 + \lambda \boldsymbol{u}_1 + O(\lambda^2)$, in the following way:

$$\boldsymbol{X}_{1t} = \boldsymbol{u}_0, \quad \boldsymbol{X}_{2t} = \boldsymbol{u}_1 + (\boldsymbol{X}_1 \cdot \nabla)\boldsymbol{u}_0, \tag{6.2a, b}$$

where $\boldsymbol{x} = \boldsymbol{X}_0$. Equation (6.2*a*) is easily integrated and substituted into (6.2*b*), which contains both periodic and steady components. We seek the time average of (6.2*b*) over one oscillation cycle, which yields the steady Lagrangian drift $\boldsymbol{X}_{2t}^{\mathrm{s}}$.

For the case of $\alpha \leqslant O(1)$ in §4, the x-direction component is plotted in figures (3*a*, *b*), which correspond to figures (1*a*, *b*) respectively. We observe in figure (3*a*) that the low-frequency Lagrangian drift correlates qualitatively with the Eulerian result; that is, there are two streams which flow toward the channel's larger end near the midline and the smaller end near the wall. Their speeds increase with α. In figure (3*b*) we again note the appearance of two crossover points and three streams, but their locations are different from figure (1*b*). For the case of $\alpha \gg 1$ (§5) the corresponding Lagrangian drift is plotted in figure 4. There are some major differences between this result and those in figure 2. We expect the two results to be similar for small particle displacements such as those nearest the wall, and indeed they are. However, the negative Lagrangian jet near the wall occupies a greater fraction of the drift layer. Farther away, the positive Lagrangian drift region is weak compared to the negative jet, unlike the Eulerian result. However, the curve asymptotes to a slow negative core drift as before. Clearly the Lagrangian profile does not integrate to zero over the cross-section, as required in the Eulerian profile. This seems to be a point of confusion in Haselton and Scherer's work. Nevertheless, the results of this section compare favourably with their Y-tube experiments, which vary α and the Reynolds number. In the present theory $R_{\mathrm{s}} = A\alpha^2$, and the channel's wider end corresponds to the direction of their daughter tubes. Although their tubes are not tapered, the transition region from parent to daughters represents an increase in total cross-sectional area. The axial velocity profiles in this region, at least in steady measurements by Schroter & Sudlow (1969) and Schreck & Mockros (1970), behave similarly to the channel model with blunted profiles during negative flow and cupped profiles with positive flow. The experiments show steady bidirectional drift for three ranges of α and R_{s}. In their low range ($\alpha = 0.68$, $R_{\mathrm{s}} = 2.6$) the observed drift is consistent with typical curves in figure (3*a*). In their middle range ($\alpha = 4.8$, $R_{\mathrm{s}} = 44$) this pattern appears to continue, but in their high range ($\alpha = 19$, $R_{\mathrm{s}} = 1400$) the streaming in the core reverses to become negative in the parent tube and blunt with a second region near the wall which is also negative but faster (their figure 5*c*). This is similar to figure 4 for large α and R_{s}. The strong swirl motions encountered in the experiment in this range are not included in our simple model, so further comparisons are difficult to make. However, the qualitative features of the model and the experiments agree as α varies from lower to higher values.

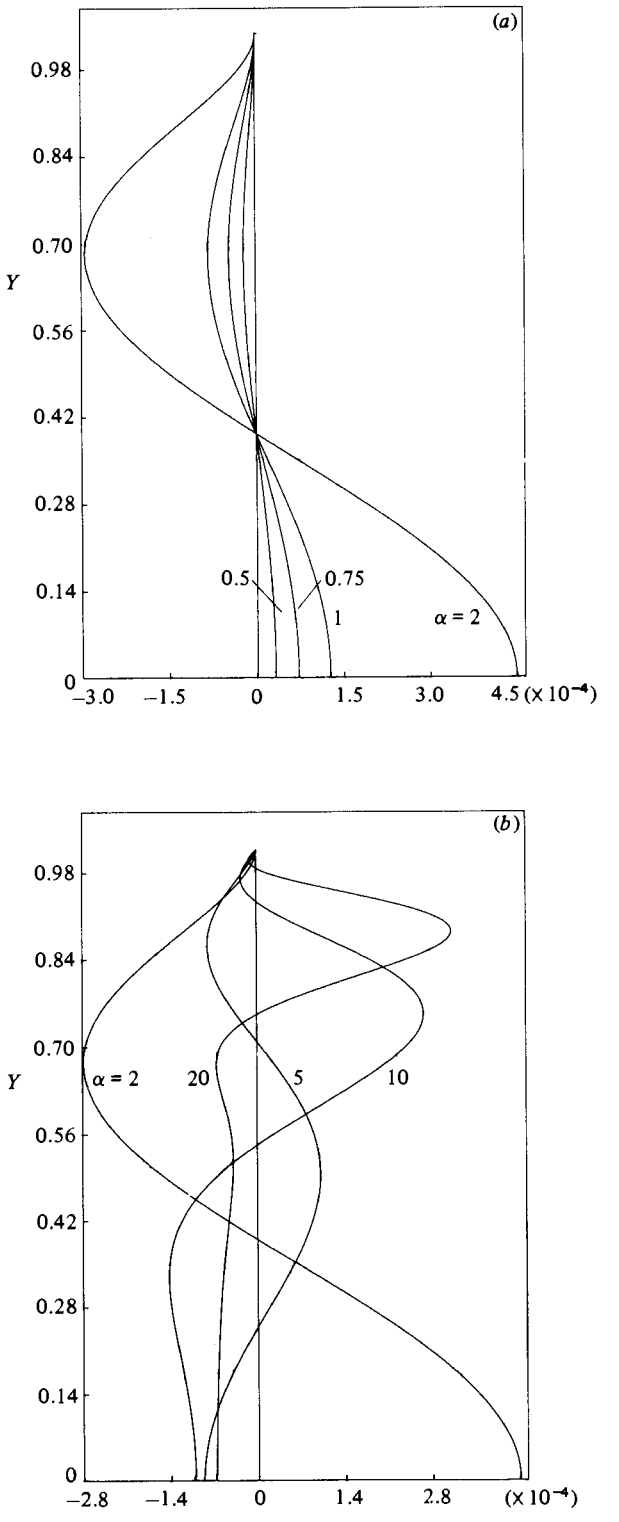

FIGURE 3. Lagrangian axial drift-velocity profile corresponding to figure 1.

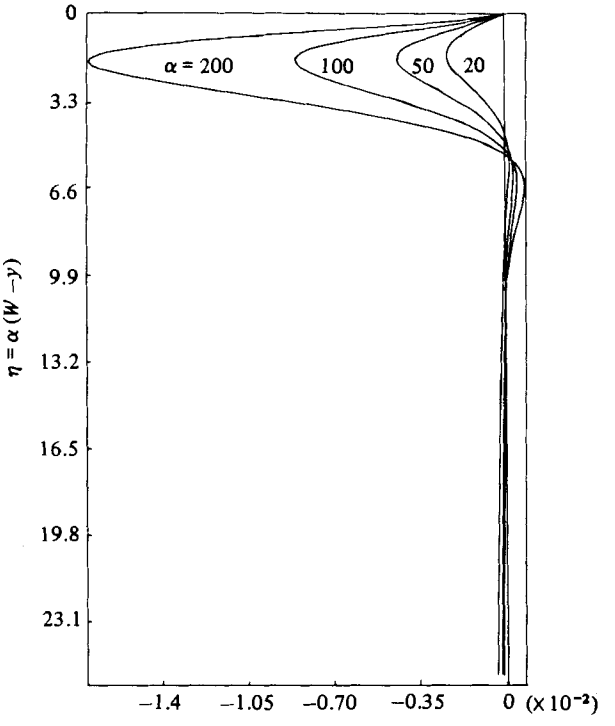

FIGURE 4. Lagrangian axial drift-velocity profile corresponding to figure 2.

7. The pressure gradient

In many theories of oscillating flow in tubes the pressure gradient is chosen to be periodic with constant amplitude. In the present theory the pressure field must adjust itself to the imposed volume cycling. When the tube or channel is tapered we expect both steady and unsteady pressure components whose amplitudes will vary with the parameters α, ϵ and A. After substituting (3.9) into (3.2) and then into (2.3), the steady pressure gradient for the $\alpha = O(1)$ solution is found to be

$$p_x^{\mathrm{s}} = \lambda\left\{\frac{1}{\alpha}2\psi_{1yyy}^{\mathrm{s}} - \langle\psi_{0y}\psi_{0xy} - \psi_{0x}\psi_{0yy}\rangle\right\}, \tag{7.1}$$

where the angle brackets indicate time average over one period. Because p_x^{s} is independent of y, we simplify (7.1) by setting $y = W(x)$, where $\psi_{0x} = \psi_{0y} = 0$. Therefore we find that the steady pressure gradient has form

$$p_x^{\mathrm{s}} = \frac{\lambda}{\alpha}2\psi_{1yyy}^{\mathrm{s}} \quad \text{on} \quad y = W(x), \tag{7.2}$$

and upon substituting (3.9) into (7.2) we arrive at the desired result. It is straightforward but tedious to show that $p_x^{\mathrm{s}} > 0$ when $W' > 0$. In the high-frequency case $\alpha \gg 1$, (5.4*b*) yields a similar but more obvious relationship to the wall slope:

$$P_x^{\mathrm{s}} = \frac{3W'}{16W^3} + \text{c.c.} \tag{7.3}$$

The steady component of pressure is larger at the wider end of the channel. This is consistent with the steady negative drift in the inviscid region at high frequency. Indeed (7.3) may be found directly from inviscid analysis using Euler's equation. Equations (7.2) and (7.3) may be rearranged to show that the dimensional steady pressure gradient increases with frequency, which is consistent with the experiments discussed in §1. This is an important practical point in HFV, since one of its attractive medical features is the small amplitude of its unsteady pressure excursions. This is desirable to minimize the detrimental effects that increased intrathoracic pressure can have on cardiac output, on the risk of lung rupture and on ventilation–perfusion matching. The experiments and theory seem to indicate that increases in steady, intrathoracic pressure with increasing α or λ is an inherent characteristic of the airway geometry. In addition, the magnitude of the unsteady pressure gradient is proportional to ω^2. Therefore the absolute pressure oscillations in the alveoli may be large. To avoid complications, such HFV devices could simply lower mean airway pressure as frequency increases.

8. Conclusions

We have examined oscillating viscous flow in a two-dimensional channel section with gradually increasing depth. The fluid motion is volume-cycled and the system is analysed in a general way, but with particular attention to modelling certain aspects of ventilation. Because the alternating velocity profiles and accelerations are different, fluid particles experience an induced steady axial drift and steady pressure gradient. The predicted Lagrangian axial drift-velocity profile is qualitatively similar to experiments on branched tubes as α varies from small to large values. The latter theory reveals the emergence of a drift layer which is much thicker than the Stokes layer. The steady pressure gradient agrees qualitatively with measurements and gross observations of tube and animal experiments during HFV. The importance of these results in terms of enhancing gas exchange remains to be shown, theoretically. However, experiments on dispersion by Tarbell, Ultman & Durlofsky (1982) and by Kamm *et al.* (1983) indicate substantial improvement of transport during oscillatory flow in a network of branching tubes compared to a single straight tube, as in Joshi *et al.* (1983). It has been customary to reduce such experimental data in terms of an effective diffusivity D_{eff}, which appears in theoretical analyses if dispersion in straight pipes under steady (Taylor 1953) or unsteady (Chatwin 1975) conditions. The parameter D_{eff} arises from integrating the convection–diffusion equation over the tube cross-section and arriving at a simplified theory for area-averaged velocity and concentration variables. Theories of HFV by Fredberg (1980) and Slutsky *et al.* (1980) rely on this approach. In the present case of a tapered conduit, however, such integration in the Eulerian frame may eliminate the bi-directional streaming effects, a rather serious defect of the averaging method.†

In the tube experiments and in the present analysis the steady axial drift nearest the wall flows toward the parent tube or smaller channel end for all values of α. The corresponding wall shear, then, is directed 'mouthward'. An important feature of airways is their mucus lining which is continually cleared by ciliary mechanisms. It appears that HFV may have the potential to facilitate mucus clearance based on the wall shear. This would be helpful in disease states where clearance is impaired.

† For example, the concentration C of a diffusible substance may be expanded as $C = C_0 + \lambda C_1 + \lambda^2 C_2 + O(\lambda^3)$. The leading term C_0 can be independent of y, so integration of uC_x and vC_y across the channel would cancel the streaming effects.

The analysis presented here assumes laminar flow conditions for all frequencies. Since no experiments on this problem in tapered channels have appeared, it is difficult to know what value of R_s will be critical. There are at least two considerations, the stability of the oscillating flow and that of the steady drift. The steady profiles in figures 1 and 2 indicate one or two inflection points over a half-width. This would tend to promote instability in the steady component coupled with the fact that the positive drift is against an adverse pressure gradient. The oscillatory component, on the other hand, may be more stable since it is primarily a Stokes-layer phenomenon.

The author wishes to thank Professors S. Rosenblat and S. H. Davis for their critical review of this manuscript. Technical assistance was provided by Mr D. Gaver, whose help is appreciated. This work was supported in part by NIH grant 1-R23-HL/GM-30574-01 and by NSF grant DME-8105822.

REFERENCES

Bohn, D. J., Miyasaka, K., Marchak, E. B., Thompson, W. K., Froese, A. B. & Bryan, A. C. 1980 Ventilation by high-frequency oscillation. *J. Appl. Physiol.: Respirat. Environ. Exercise Physiol.* **48**, 710–716.

Butler, W. J., Bohn, D. J., Bryan, A. C. & Froese, A. B. 1980 Ventilation by high-frequency oscillation in humans. *Anesth. Analg.* **59**, 577–584.

Chatwin, P. C. 1975 On the longitudinal dispersion of passive contaminant in oscillatory flows in tubes. *J. Fluid Mech.* **71**, 513–527.

Fettis, H. E. 1956 On the integration of a class of differential equations occurring in boundary-layer and other hydrodynamic problems. In *Proc. 4th Midwest Conf. Fluid Mech., 1955, Purdue University*, pp. 13–114.

Fredberg, J. J. 1980 Augmented diffusion in the airways can support pulmonary gas exchange. *J. Appl. Physiol.: Respirat. Environ. Exercise Physiol.* **49**, 232–238.

Grotberg, J. B. 1983*a* Oscillatory flow in a tapered channel. *Biomech. Symp., Proc. Amer. Soc. Mech. Engng.*

Grotberg, J. B. 1983*b* Mechanisms of gas transport in high-frequency ventilation. *Proc. Ann. Conf. Engng Med. Biol.*

Hall, P. 1974 Unsteady viscous flow in a pipe of slowly varying cross-section. *J. Fluid Mech.* **64**, 209–226.

Haselton, F. R. & Scherer, P. W. 1982 Flow visualization of steady streaming in oscillatory flow through a bifurcating tube. *J. Fluid Mech.* **123**, 315–333.

Horsfield, K. & Cumming, G. 1967 Angles of branching and diameters of branches in the human bronchial tree. *Bull. Math. Biophys.* **29**, 245–259.

Jones, A. F. & Rosenblat, S. 1968 The flow induced by torsional oscillations of infinite planes. *J. Fluid Mech.* **37**, 337–347.

Joshi, C. H., Kamm, R. D., Drazen, J. M. & Slutsky, A. S. 1983 An experimental study of gas exchange in laminar oscillatory flow. *J. Fluid Mech.* **133**, 245–254.

Kamm, R. D., Collins, J., Whang, J., Slutsky, A. S. & Greiner, M. 0000 Gas transport during oscillatory flow in a network of branching tubes (submitted).

McEvoy, R. D., Davies, J. H., Mannino, F. L., Prutow, R. J., Schumacker, P. T., Wagner, P. D. & West, J. B. 1982 Pulmonary gas exchange during high-frequency ventilation. *J. Appl. Physiol.: Respirat. Environ. Exercise Physiol.* **52**, 1278–1287.

Scherer, P. W. & Haselton, F. R. 1982 Convective exchange in oscillatory flow through bronchial-tree models. *J. Appl. Physiol.: Respirat. Environ. Exercise Physiol.* **53**, 1023–1033.

Schreck, R. M. 1972 Laminar flow through bifurcations with applications to the human lung. Ph.D. dissertation. Northwestern University, Evanston, Illinois.

Schreck, R. M., Mockros, L. F. 1970 Fluid dynamics in the upper pulmonary airways. *3rd Fluid Plasma Dyn. Conf., Los Angeles; AIAA Paper* 70–788.

Schroter, R. C. & Sudlow, M. F. 1969 Flow patterns in models of the human bronchial airways. *Respirat. Physiol.* **7**, 341–355.

SIMON, B., WEINMANN, G. & MITZNER, W. 1982 Significance of mean airway pressure during high frequency ventilation. *The Physiologist* **25** (4), 282.

SLUTSKY, A. S., DRAZEN, J. M., INGRAM, R. H., KAMM, R. D., SHAPIRO, A. H., FREDBERG, J. J., LORING, S. H. & LEHR, J. 1980 Effective pulmonary ventilation with small-volume oscillations at high frequency. *Science* **209**, 609–611.

STUART, J. T. 1966 Double boundary layers in oscillatory viscous flow. *J. Fluid Mech.* **24**, 673–687.

TARBELL, J. M., ULTMAN, J. S. & DURLOFSKY, L. 1982 Oscillatory convective dispersion in a branching tube network. *Trans. ASME* K: *J. Biomech. Engng* **104**, 338–342.

TAYLOR, G. I. 1953 Dispersion of soluble matter in solvent flow slowly through a tube. *Proc. R. Soc. Lond.* A **219**, 186–203.

WEIBEL, E. R. 1963 *Morphometry of the Human Lung.*